



HAL
open science

Coexisting magnetic structures and spin reorientation in Er 0.5 Dy 0.5 FeO 3 : Bulk magnetization, neutron scattering, specific heat, and density functional theory studies

Sarita Rajput, Padmanabhan Balasubramanian, Ankita Singh, Françoise
Damay, C M N Kumar, W. Tabis, T. Maitra, V K Malik

► To cite this version:

Sarita Rajput, Padmanabhan Balasubramanian, Ankita Singh, Françoise Damay, C M N Kumar, et al.. Coexisting magnetic structures and spin reorientation in Er 0.5 Dy 0.5 FeO 3 : Bulk magnetization, neutron scattering, specific heat, and density functional theory studies. *Physical Review B*, 2022, 105 (21), pp.214436. 10.1103/PhysRevB.105.214436 . hal-04252080

HAL Id: hal-04252080

<https://hal.science/hal-04252080>

Submitted on 20 Oct 2023

HAL is a multi-disciplinary open access archive for the deposit and dissemination of scientific research documents, whether they are published or not. The documents may come from teaching and research institutions in France or abroad, or from public or private research centers.

L'archive ouverte pluridisciplinaire **HAL**, est destinée au dépôt et à la diffusion de documents scientifiques de niveau recherche, publiés ou non, émanant des établissements d'enseignement et de recherche français ou étrangers, des laboratoires publics ou privés.

Coexisting magnetic structures and spin-reorientation in $\text{Er}_{0.5}\text{Dy}_{0.5}\text{FeO}_3$: Bulk magnetization, neutron scattering, specific heat, and *Ab-initio* studies

Sarita Rajput,¹ Padmanabhan Balasubramanian,² Ankita Singh,¹ Francoise Damay,³ C.M.N. Kumar,^{4,5} W. Tabis,⁵ T. Maitra,¹, V. K. Malik^{1,*}

¹*Department of Physics, Indian Institute of Technology Roorkee, Roorkee 247 667, India*

²*Department of Physics, Graphic Era University, Dehra Dun, Uttarakhand 248 002, India*

³*Laboratoire Léon Brillouin, CEA-CNRS, CEA/Saclay, 91191 Gif sur Yvette, France*

⁴*Institute of Solid State Physics, Vienna University of Technology, Wiedner Hauptstrasse 8-10, 1040 Wien, Austria*

⁵*AGH University of Science and Technology,*

Faculty of Physics and Applied Computer Science, 30-059 Kraków, Poland

(Dated: October 5, 2021)

Abstract

The complex magnetic structures, spin-reorientation and associated exchange interactions have been investigated in $\text{Er}_{0.5}\text{Dy}_{0.5}\text{FeO}_3$ using bulk magnetization, neutron diffraction, specific heat measurements and density functional theory calculations. The Fe^{3+} spins order as G-type antiferromagnet structure depicted by $\Gamma_4(G_x, A_y, F_z)$ irreducible representation below 700 K, similar to its end compounds. The bulk magnetization data indicate occurrence of the spin-reorientation and rare-earth magnetic ordering below ~ 75 K and 10 K, respectively. The neutron diffraction studies confirm an “incomplete” $\Gamma_4 \rightarrow \Gamma_2(F_x, C_y, G_z)$ spin-reorientation initiated ≤ 75 K. Although, the relative volume fraction of the two magnetic structures varies with decreasing temperature, both co-exist even at 1.5 K. Below 10 K, magnetic ordering of $\text{Er}^{3+}/\text{Dy}^{3+}$ moments in c_y^R arrangement develops, which gradually increases in intensity with decreasing temperature. At 2 K, magnetic structure associated with c_z^R arrangement of $\text{Er}^{3+}/\text{Dy}^{3+}$ moments also appears. At 1.5 K the magnetic structure of Fe^{3+} spins is represented by a combination of $\Gamma_2 + \Gamma_4 + \Gamma_1$, while the rare earth magnetic moments’ order coexists as c_y^R and c_z^R corresponding to Γ_2 and Γ_1 representation, respectively. The observed Schottky anomaly at 2.5 K suggests that the “rare-earth ordering” is induced by polarization due to Fe^{3+} spins. The $\text{Er}^{3+}-\text{Fe}^{3+}$ and $\text{Er}^{3+}-\text{Dy}^{3+}$ exchange interactions, obtained from first principle calculations, indicate that these interactions primarily cause the complicated spin-reorientation and c_y^R rare-earth ordering in the system, respectively, while the dipolar interactions between rare-earth moments, result in the c_z^R type rare-earth ordering at 2 K.

PACS numbers: 75.25.-j, 75.47.Lx, 75.30.Gw, 71.20.-b

I. INTRODUCTION

Rare-earth orthoferrites materials $R\text{FeO}_3$ (R = rare-earth ion), have shown potential for technologically relevant applications via observation of spin switching, spontaneous exchange bias and optically controlled ultrafast spin dynamics[1–7]. Additional important properties include large linear magneto-dielectric effect, spontaneous ferroelectric polarization, multiferroicity, and magnetocaloric effect[8–13].

The orthoferrites materials belong to the family of perovskites and crystallize in the structure represented by orthorhombic space group $D_{16}^{2h} \cdot Pbnm$ symmetry, as observed in case of manganite and cobaltate materials[14, 15]. Unlike manganites, long-range static Jahn-Teller effect is absent in orthoferrites [14]. The FeO_6 octahedra in rare-earth orthoferrites possess a GdFeO_3 type distortion with nearly equal Fe-O bond lengths[16–20]. The structural distortion increases with atomic number of R [21].

The rare-earth orthoferrites ($R\text{FeO}_3$) are antiferromagnets with a Néel temperature(T_{N1}) in the temperature range of 650-760 K[22, 23]. Increase in the atomic number of R results in systematic reduction of

T_{N1} [23]. At T_{N1} , the orthoferrites undergo transition from paramagnetic to G-type anti-ferromagnetic state with ordering wave-vector $\vec{k}=(0, 0, 0)$. The magnetic structure belongs to Γ_4 irreducible representation, which can be written as (G_x, A_y, F_z) in Bertaut notation[24]. The Fe^{3+} spins order primarily in antiferromagnetic G-type configuration along the crystallographic a -axis(G_x), while A_y and F_z correspond to the A-type antiferromagnetic and ferromagnetic arrangement of the spins along the crystallographic b and c -axes due to covert and overt canting, respectively[23, 25, 26].

The dominant interaction in all the orthoferrite compounds is an isotropic $\text{Fe}^{3+}-\text{Fe}^{3+}$ super-exchange interaction which is denoted as $J_{\text{Fe-Fe}}$. The additional isotropic interactions are the $R^{3+}-\text{Fe}^{3+}$ and $R^{3+}-R^{3+}$ interactions[25]. The strength of the isotropic interactions are in the following order, $J_{\text{Fe-Fe}} > J_{R-\text{Fe}} > J_{R-R}$. The anti-symmetric Dzyaloshinski-Moriya interaction is responsible for the covert and overt magnetic orderings (A_y, F_z) due to small canting of the Fe^{3+} spins. Yamaguchi *et al.*[25] also discussed the role of anisotropic parts of $R^{3+}-\text{Fe}^{3+}$ exchange interactions, which are responsible for the spin reorientation in orthoferrites.

NdFeO_3 is one of the most studied orthoferrite compound for magnetic ordering and spin reorientation process[16, 22, 23, 25–32] in which the Fe^{3+} spins undergo a continuous $\Gamma_4 \rightarrow \Gamma_2(F_x, C_y, G_z)$ reorientation be-

* vivek.malik@ph.iitr.ac.in

tween 200 and 150 K [28, 30, 33]. In the Γ_2 magnetic structure, the crystallographic c -axis is the easy axis of the ordered Fe^{3+} spins in basic G-type antiferromagnetic configuration along with ferromagnetic F_x and antiferromagnetic C_y configurations due to overt and covert canting of the spins[24, 25]. The Nd^{3+} - Fe^{3+} interactions leads to polarization of the Nd^{3+} magnetic moments, which result in their long range ordering at liquid He temperatures[26, 29, 34]. In most of the orthoferrites (except DyFeO_3), the R^{3+} -moments usually order in a structure which is symmetry-compatible with the G-type arrangement of Fe^{3+} spins[25]. For instance, in NdFeO_3 , the Nd^{3+} moments order as c_y^R , compatible to the Γ_2 representation of Fe^{3+} spins[26, 29, 34]. At the lowest temperatures (usually below 2 K) the Nd^{3+} - Nd^{3+} interactions begin to supercede the Nd^{3+} - Fe^{3+} interactions, resulting in long-ranged independent ordering of the Nd^{3+} moments, which can be considered as Landau-type second order phase transition [35].

Another isostructural, but relatively less studied, orthoferrite, ErFeO_3 , shows magnetic properties similar to NdFeO_3 . Fe^{3+} spins in ErFeO_3 order as canted G-type antiferromagnet in Γ_4 representation below 620 K (T_{N1})[22]. Between $\sim 100/110$ K and $\sim 80/90$ K, the Fe^{3+} spins undergo a $\Gamma_4 \rightarrow \Gamma_2$ type gradual spin reorientation [36–40]. The isotropic and anisotropic Er^{3+} - Fe^{3+} exchange interactions result in polarization of the Er^{3+} moments which causes the spin reorientation of Fe^{3+} spins.

In the low temperature phase (below 20 K), the magnetic arrangement of Fe^{3+} spins is more complex due to the influence of Er^{3+} ordering on Fe^{3+} magnetic structure. Koehler *et al.*[22] proposed that the magnetic ordering of Fe^{3+} spins, below rare-earth ordering temperature, could be given by a G-type antiferromagnetic structure with Fe^{3+} spins confined in a - b plane. At 1.3 K, Er^{3+} moments ordered in a magnetic structure given by C_z configuration[22]. Based on neutron diffraction data, Gorodetsky *et al.*[41] proposed the possibility of two the Fe^{3+} magnetic structure below the Er^{3+} ordering temperature. First magnetic structure was given by mixed representation of G_{xy} with Fe^{3+} spins aligned in ab plane at an angle of $33^\circ \pm 4^\circ$ from the b axis. As per the second proposed magnetic structure, Fe^{3+} spins should order as G -type structure in bc plane (G_{yz}) with the spins at an angle of $51^\circ \pm 8^\circ$ from the b axis. Based on magnetization and torque measurements of the same study[41], Gorodetsky *et al.* confirmed the existence of G_{yz} magnetic structure for Fe^{3+} spins at $T < 4.5$ K. The low temperature magnetic structure of Fe^{3+} moments remained unresolved for long time. Recently, Deng *et al.*[8] confirmed with the help of neutron diffraction and symmetry analysis that the low temperature magnetic structure of Fe^{3+} remains Γ_2 below spin reorientation temperature. Additionally Deng *et al.* also detected C_y (C_x in $Pnma$ space group) mode of $\Gamma_2(F_x, C_y, G_z)$ magnetic structure below 5 K, at which, the Er^{3+} moments start to arrange in the long range antiferromagnetic ordering given by c_z^R (c_y^R in $Pnma$ space group) configuration[8, 41]. The

concurrency of centro-symmetric space group of Fe^{3+} sublattice along with centro-asymmetric space group of Er^{3+} opens the possibility of improper polarization along with magnetic ordering and hence multiferroicity in ErFeO_3 [8]. Yokota *et al.* [11] observed the coexistence of ferroelectricity and magnetism in ErFeO_3 thin films by modification of structure from orthorhombic to hexagonal via yttria stabilized zirconia substrate.

In the family of orthoferrites, the DyFeO_3 exhibits an exceptional trend in spin-reorientation and rare-earth ordering[10, 36, 42–45]. Below T_{N1} (~ 650 K), the Fe^{3+} moments order with a structure given by Γ_4 representation. However, near ~ 35 K, a $\Gamma_4 \rightarrow \Gamma_1(A_x, G_y, C_z)$ type spin reorientation occurs where antiferromagnetic axis (b axis) becomes parallel to Dzyaloshinsky-Moriya vector and weak ferromagnetic component cease to exist due to a pure uncanted antiferromagnetic structure[42, 43]. This transition, also known as Morin transition, is unique for DyFeO_3 in the family of rare-earth orthoferrites[23, 36, 42, 46, 47].

Below $T_{N2} \sim 4$ K, due to the Dy^{3+} - Dy^{3+} exchange and dipole interactions, the Dy^{3+} moments arrange in the $\Gamma_5(G_x^R, A_y^R)$ configuration making an angle of 30° with the b axis [23, 42, 48–50]. Iso-structural Dy-based compounds viz. DyAlO_3 [51] and DyCrO_3 [52], also arrange in the same configuration. Due to large single ion anisotropy, the Dy^{3+} moments are confined to the a - b plane[53].

Prelorendjo *et al.*[43] also studied magnetic field induced spin reorientation. At 4.2 K, $\Gamma_1 \rightarrow \Gamma_4$, $\Gamma_1 \rightarrow \Gamma_2$, and $\Gamma_1 \rightarrow \Gamma_4$ type spin reorientations of the Fe^{3+} sublattice were observed in DyFeO_3 on application of external magnetic field along b , a , and c -axis of the crystal, respectively[43]. The (G_x^R, A_y^R) arrangement of Dy^{3+} moments, is not symmetry compatible with the field induced Γ_2 magnetic structure of the Fe^{3+} sub lattice[47]. Co-existence of two incompatible magnetic structures breaks the inversion symmetry which is essential for linear magneto-electric effect[47, 54]. Experimentally, a linear magneto-electric tensor component with a value as large as 2.4×10^{-2} esu is observed below the Dy^{3+} antiferromagnetic ordering temperature[10]. Interestingly, large ferroelectric polarization along with magnetic ordering also is achieved by application of an external magnetic field along the c axis of DyFeO_3 [10, 44, 55]. Rajeswaran *et al.*[55] claimed to observe simultaneous ferroelectricity and weak ferromagnetism above Morin transition temperature in polycrystalline DyFeO_3 . Recent study by Wang *et al.*[45] observed a long- to short-range ordering transition of Dy^{3+} concurrent to the magnetic field (along the c -axis) induced spin reorientation of the Fe^{3+} sublattice. The magnetic field induced short range ordering of the Dy^{3+} moments is responsible for the observed multiferroic phase induced by external magnetic field [10, 45]

In addition to the pure orthoferrites, doping and/or substitution at the Fe and/or R sites shows interesting variations in the structural, magnetic, and electronic properties, while the fundamental characteristic of ortho-

ferrites is still retained[12, 56–61]. For instance, doping at the Fe-site with Mn has been studied and resulted in a systematic decrease of the Néel temperature[56, 61], structural distortion due to Jahn-Teller effect[62], and modifies the preferred direction of Fe^{3+} spins due to single ion anisotropy of Mn^{3+} ions[56, 63]. Substitution at A-site by another rare-earth though does not affect the structural behaviour and Néel temperature, but however affects the spin-reorientation and the rare-earth ordering[60]. For instance, two-fold spin-reorientations are observed in single crystals of $\text{Dy}_{0.5}\text{Pr}_{0.5}\text{FeO}_3$ and $\text{Ho}_{0.5}\text{Dy}_{0.5}\text{FeO}_3$ with varying temperature and magnetic field[60, 64]. However, in these cases, the nature of the rare-earth ordering and its effect on the spin reorientation are not known.

Considering the striking contrast in the nature of Fe^{3+} and R^{3+} -orderings in ErFeO_3 and DyFeO_3 , it would be interesting to explore the properties of $\text{Er}_{0.5}\text{Dy}_{0.5}\text{FeO}_3$ (EDFO). A very complex interplay of the various exchange interactions between the $\text{Er}^{3+}/\text{Dy}^{3+}$ and Fe^{3+} sub lattices along with the $R^{3+}-R^{3+}$ exchange is expected. Additionally, due to the large magnetic moments of both the rare-earths, the classical dipole interactions are expected to play a prominent role in determining the complex ground state magnetic orders at the lowest temperatures. Due to large differences in the nature of single ion anisotropy of both the rare-earth ions (Er^{3+} and Dy^{3+}) which can compete with the exchange and dipolar interactions, it would also be interesting to establish, whether the rare-earth ordering in the system is long-ranged, or magnetic ground state turns into a spin-glass. Additionally, the possibility of a magneto-electric effect is also worth exploring.

Thus, we have experimentally studied the bulk magnetization, heat capacity, neutron diffraction and magneto-dielectric measurements of polycrystalline EDFO. Theoretically, density functional theory calculations are performed to understand the ground state electronic structure and evaluate the various exchange interactions from the total energies of various possible magnetic configurations.

II. METHODS

A. Experimental

Polycrystalline samples of EDFO were synthesized using solid state reaction method. Er_2O_3 , Dy_2O_3 , and Fe_2O_3 precursor powders were weighed in appropriate stoichiometry and ground in an agate mortar for 12 hours. The steps involved calcination at 1200°C for 24 hrs, followed by heating at 1350°C for 24 hrs with intermediate grinding. Crystal structure of the sample was identified using a Bruker D8 two circle powder x-ray diffractometer with $\text{Cu } K_\alpha$ source. Bulk magnetization measurements were performed using SQUID magnetometer of Quantum Design Inc.’s Magnetic Proper-

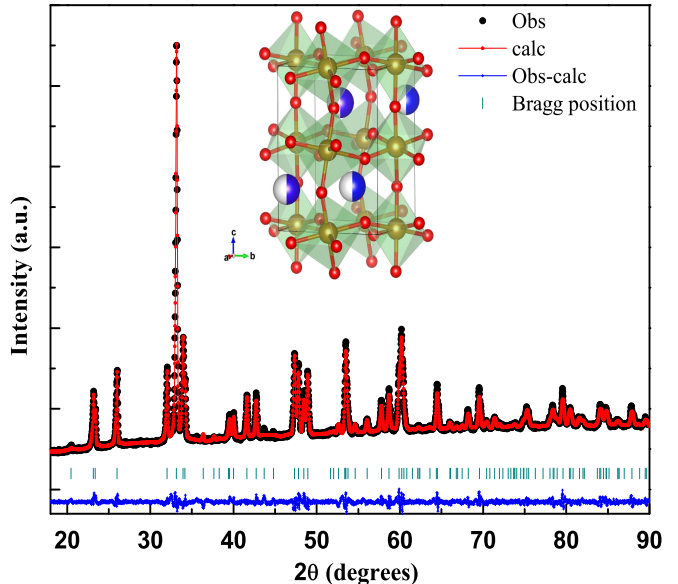


FIG. 1. (color online) Observed and refined x-ray diffraction pattern of EDFO at room temperature. We also show the unit cell of EDFO, wherein the Er and Dy atoms occupy same crystallographic site. The Er/Dy, Fe and O atoms are represented by Silver/blue, green and red spheres, respectively, in the unit cell.

ties Measurement System-XL (QD-MPMS-XL) and vibrating sample magnetometer option of Quantum Design Inc.’s Dynacool Physical Properties Measurement System (QD-PPMS). Zero field cooled (ZFC) and field cooled (FC) magnetization measurements were carried out from 300 K to 1.5 K in the presence of 0.01 and 0.1 T magnetic field. $M-H$ isotherms were measured at various temperatures between 300 and 1.5 K. Using custom designed probe for QD-PPMS and Hioki EIM3536 LCR meter, magneto-dielectric studies were carried out in the temperature range of 300-2 K, at frequencies ranging from 1 kHz to 500 kHz in the external magnetic field of 0, 0.1 and 1 Tesla. Heat capacity measurements were performed using the QD-PPMS with ^3He option in the temperature range 20-0.4 K and magnetic field values of 0, 2 and 5 T. Powder Neutron diffraction studies in zero magnetic field were carried out at various temperatures between 300-1.5 K to identify the crystal as well as magnetic structure and their evolution as a function of temperature. The neutron diffraction measurements were performed at powder diffractometer G-41-I ($\lambda = 2.4206 \text{ \AA}$), at LLB, Saclay in France. The Rietveld analysis of the diffraction data was performed using FullProf suite of programs[65, 66]. Magnetic structures were determined using the irreducible representations from BasIreps [67].

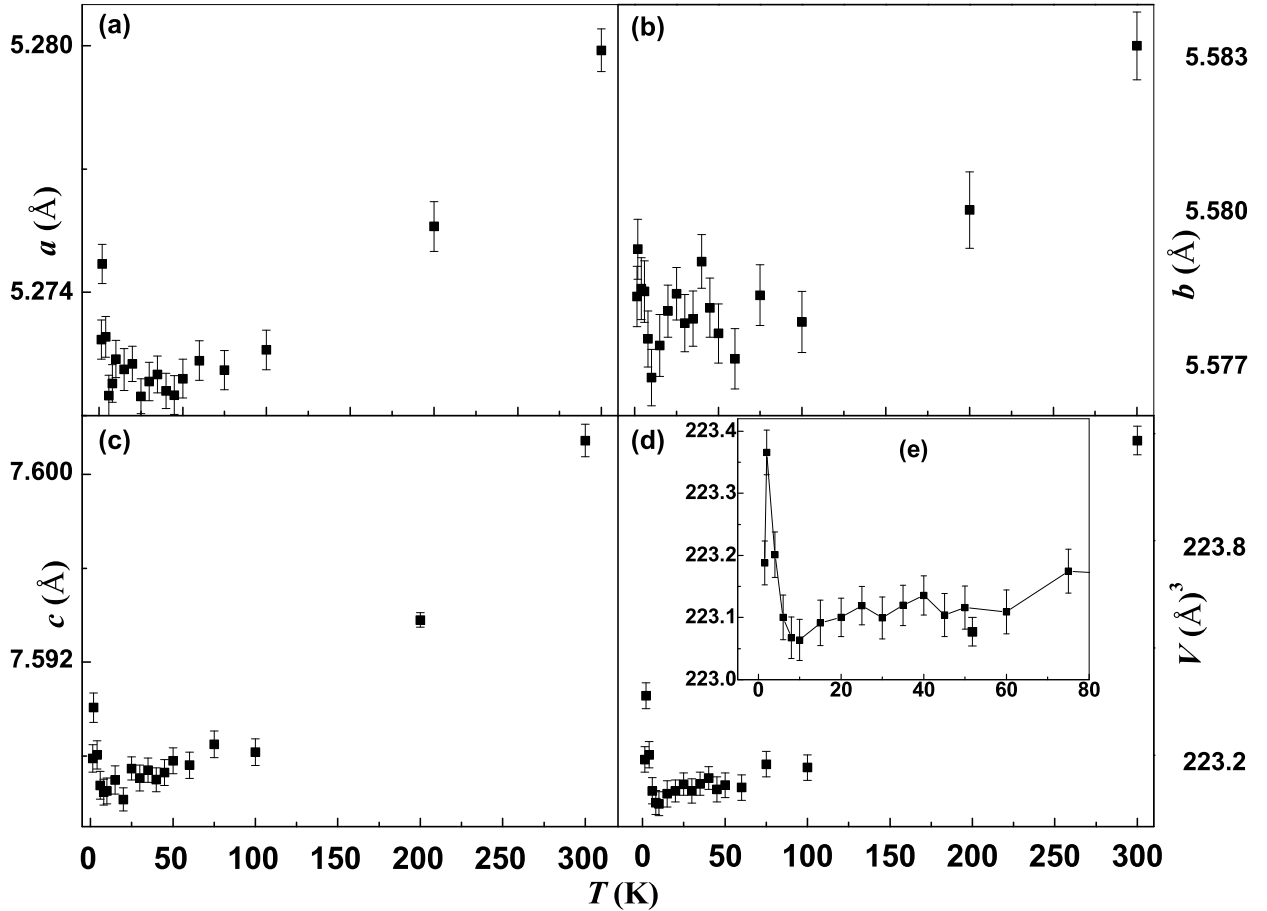


FIG. 2. (a)-(c): Temperature variation of lattice parameters, (d) unit cell volume of EDFO and (e) shows anomalous rise in volume below 10 K.

B. Theoretical

Electronic structure of EDFO was studied using density functional theory implemented in the Vienna Ab-initio simulation program (VASP) which uses the projector augmented wave (PAW) method [68]. Calculations were performed using Perdew-Burke-Ernzerhof (PBE) based generalized gradient approximation (GGA) [69] and GGA+ U [70]. A cut-off energy of 500 eV was used in the expansion of the plane waves. The structure was relaxed keeping the Er/Dy 4*f* electrons as core electrons. Ionic positions were relaxed until the forces on the ions are less than $0.1 \text{ meV } \text{ \AA}^{-1}$. For the electronic self-consistent calculations, the Er/Dy 4*f* electrons were treated as valence electrons. We have considered following orbitals in the valence band for each atom; Fe: 3*d*, 4*s*, O: 2*s*, 2*p* and Er/Dy: 4*f*, 5*p*, 5*d*, 6*s*. A $6 \times 6 \times 6$ Monkhorst-Pack k -mesh centered at Γ point in Brillouin zone was used for performing the Brillouin zone integrations.

III. EXPERIMENTAL RESULTS

A. Structural Characterization

Fig. 1 shows the room temperature powder x-ray diffraction pattern for EDFO. The pattern is refined by Rietveld method using Fullprof program. The pattern is refined to a single phase, with no trace of any impurity or unreacted phases. The compound crystallizes in the orthorhombic $Pbnm$ space group. At room temperature, the estimated lattice parameters are $a=5.2793 \text{ \AA}$, $b=5.5835 \text{ \AA}$ and $c=7.6011 \text{ \AA}$. The lattice (structural) parameters were also extracted from neutron powder diffraction patterns collected between 300 to 1.5 K. In Fig. 2(a-c), the temperature variation of the three lattice parameters is shown. As expected, a , b , and c continuously decrease from 300 till 100 K. Further till 10 K, a and c decrease gradually with temperature, while b shows a “hump” like feature between 50 and 10 K. Below 5 K we observe a sharp increase in all the three lattice parameters with a maximum around 2 K. The temperature variation of unit cell volume V (Fig. 2(d)) is similar to that of a and c , with a slope change below 100 K. In the Fig. 2(e),

we observe a sharp increase in volume with a maximum value at 2 K. In the absence of structural transformation, the “isotropic” negative thermal expansion effects may be considered as magneto-elastic or magneto-volume effect[71]. The anomalous negative thermal expansion is found to be associated with rare-earth ordering.

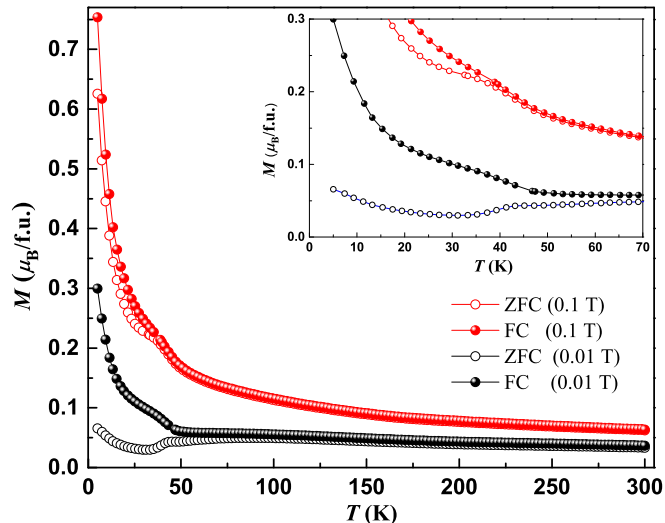


FIG. 3. (color online) ZFC-FC magnetization of EDFO at (a) 0.01 T and (b) 0.1 T. The inset shows enlarged portion of the graph below 70 K.

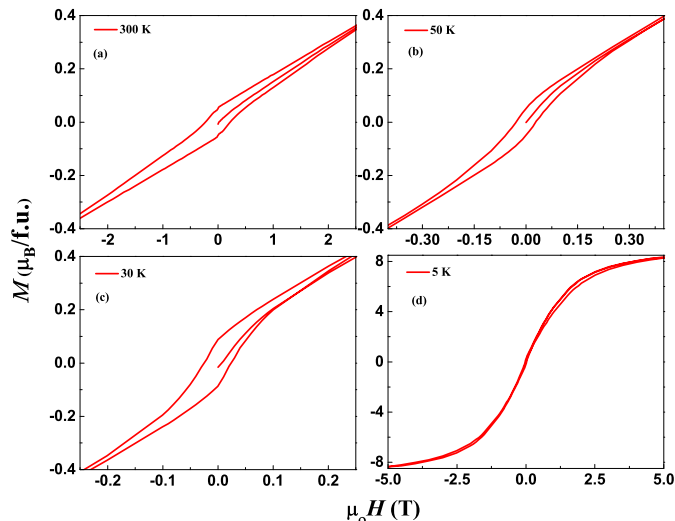


FIG. 4. (color online) M - H isotherms of EDFO at various temperatures.

B. Magnetic properties

1. DC Magnetization

Fig. 3, shows the temperature dependence zero field cooled (ZFC) and field cooled (FC) magnetization measurements for EDFO from 2 K to 300 K at magnetic fields

of 0.01 T and 0.1 T. At 300 K, EDFO is expected to be antiferromagnetically ordered in $\Gamma_4(G_x, A_y, F_z)$ magnetic structure, due to which we observe a small difference in the ZFC and FC magnetization. The spin reorientation of Fe^{3+} spins begins below $\sim 100/110$ K in ErFeO_3 [36–40]. Unlike ErFeO_3 , the signature of spin reorientation in EDFO appears below 70 K, indicated by the increase in bifurcation between ZFC-FC magnetization (in 0.01 T) as seen in Fig. 3. Near $T \sim 45$ K, the ZFC magnetization shows a drop whereas the FC magnetization increases in a continuous manner with a change in slope. Below 25 K, the ZFC magnetization rises again, similar to ErFeO_3 [72]. Unlike DyFeO_3 , signature of a clear Morin-like transition is not observed in EDFO[44]. The ZFC-FC measurements for 0.1 T is also shown in Fig. 3. With decrease in temperature, the ZFC and FC curves for 0.1 T show a continuous increase with a small slope change near 45 K.

The isothermal field variation of magnetization for various temperatures are shown in Fig. 4. At 300 K, the M - H curve shows typical hysteresis loop of a canted antiferromagnet with a coercivity of nearly 0.2 T, confirming the weak ferromagnetism in EDFO. At 50 K and 30 K, the M - H isotherm loops have relatively narrower hysteresis loops with an almost linear magnetization at higher magnetic fields. The slope of linear magnetization at higher fields, which increases with decreasing temperature, is due to the development of paramagnetic moment of both the rare-earth ions[72]. At 5 K, the non-linear behavior of the magnetization, at higher magnetic field, suggests polarization of the R^{3+} moments. In a magnetic field of 5 T, the magnetization attains a near-saturation (M_{sat}) value of nearly $8.4 \mu_B$. Both Er^{3+} and Dy^{3+} ions have a ground state angular momentum quantum number $J=15/2$ and $\sim 10 \mu_B$ magnetic moment. Magnetization studies on single crystals of DyFeO_3 reveal that the magnetic moment along b axis attains a maximum value of nearly $9 \mu_B$, while a total magnetization of $10.6 \mu_B$ is obtained. Similarly, in ErFeO_3 , the total magnetic moment reaches a value of $7.6 \mu_B$ in a magnetic field of 5 T[73]. Thus the value of M_{sat} in EDFO is close to the total magnetic moment observed in ErFeO_3 and thus smaller than the expected average magnetic moment of $\sim 10 \mu_B$.

2. Magnetic Neutron Diffraction

In this section, the magnetic structures of EDFO obtained from neutron diffraction data is discussed. At 300 K (pattern not shown), we observe the structurally forbidden (101) and (011) magnetic peaks associated with G-type magnetic ordering of the Fe^{3+} spins. The neutron diffraction patterns obtained at 200 K, 45 K and 20 K are shown in Fig. 5(a), (b), and (c). The magnetic peaks (011) and (101) correspond to ordering vector, $\vec{k}=(0,0,0)$. A ratio of nearly 1/3 between the intensities of (101) and (011) peaks confirms that the Fe^{3+} spins are arranged as G_x in Γ_4 magnetic structure at 200 K[74]. Between 200 and 100 K, the ratio between the

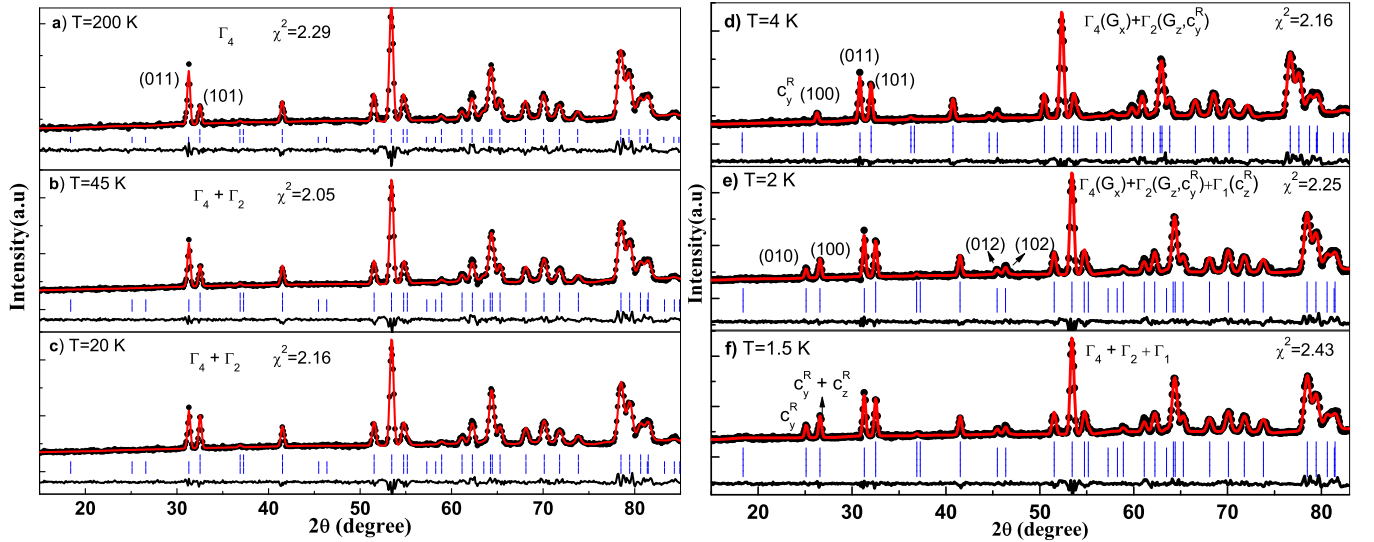


FIG. 5. Neutron powder diffraction pattern and refinements of EDFO at 200, 45 and 20 K (left panel) showing the systematic evolution of intensity of (011) and (101) magnetic peaks. In the right panel, patterns and refinement for 4, 2 and 1.5 K are shown. Additional magnetic peaks arising due to ordering of $\text{Er}^{3+}/\text{Dy}^{3+}$ moments are marked.

peaks remain nearly constant, while the absolute values of the intensity increase. Below 75 K, we observe relative increase in the intensity of (101) peak in comparison to the (011) peak, which indicates the onset of spin-reorientation (data not shown). As shown in Fig. 5b), at 45 K, the intensity of (011) peak is approximately twice in comparison to the intensity of (101) peak. Such intensity ratio suggests that a mixed magnetic structure, $G_{xz}(\Gamma_4 + \Gamma_2)$, exists at 45 K. The changes in intensity ratio of (101) and (011) peaks are much more gradual than the previously studied mixed doped orthoferrite, $\text{Nd}_{0.5}\text{Dy}_{0.5}\text{FeO}_3$ [75].

Equal intensity ratio between (101) and (011) peaks is required for a pure $\Gamma_2(G_z)$ magnetic structure[74]. As evident from Fig. 5c), the intensity of (101) and (011) peaks is not equal, hence the spin reorientation transition does not complete even at 20 K. In Fig. 5d), e), and f), the neutron diffraction patterns for 4, 2 and 1.5 K are shown. As shown in Fig. 5d), e), and f), the intensity ratio of (011) and (101) peaks remain slightly higher than 1 indicating presence of a mixed structure of Fe^{3+} sub-lattice down to the lowest measured temperature (1.5 K).

Below 10 K additional peaks near 26° and 45° develop. In the $Pbnm$ space group the peak at 26° can be indexed to (100), while the peaks near 45° can be indexed to (012) and (102). All the three peaks are structurally forbidden in $Pbnm$ space group. Development of additional peaks can be attributed to the onset of rare-earth ordering. With decrease in temperature, the intensity of the three magnetic peaks increase in a systematic manner. At 2 K, additional magnetic peak corresponding to (010) reflection appears, along with sudden increase in intensity of (100) and (012)/(102) peaks related to rare-earth ordering and (101) peak related to Fe^{3+} sub lattice or-

dering. The magnetic peaks that develop below 10 K can also be indexed to $\vec{k}=(0,0,0)$.

In Fig. 6a), the temperature variation of the integrated intensities of the (011) and (101) magnetic peaks is shown for temperature range from 300 till 1.5 K. Below 75 K, the intensity of (011) peak decreases, while that of (101) peak increases in systematic manner. Such a variation of magnetic peaks' intensity confirms the initiation of the spin reorientation at 75 K. This trend persists till 25 K, though they never crossover, which is a signature of complete reorientation. In Fig. 6b), the enlarged version of intensity variation is shown between 15 to 1.5 K. Below 15 K, the (011) peak shows a gradual increase till 4 K, while that of (101) peak remains nearly constant with small fluctuations till 4 K. The intensity of (101) peak increases considerably below 4 K. Hence, the ratio of (011) and (101) intensity decreases below 4 K.

Additionally, Fig. 6b) also shows the rise in intensity of the (100) and (010) peaks, associated with R^{3+} ordering. Between 10 and 4 K, the (100) peak shows a gradual rise in intensity. However, the (100) peak, similar to (101) peak, shows "discontinuous jump" in intensity at 4 K, which is accompanied by sudden development of (010) peak. The overall variations in intensity clearly suggests coexistence of the multiple magnetic structures due to Fe^{3+} and R^{3+} ordering.

The nature of the multiple phases in EDFO are understood in detail from magnetic structural refinements using representational analysis[76]. The Fe atom occupies the $4b$ Wyckoff position, while the R atoms occupy the $4c$ sites. The Fe^{3+} spins can arrange in four possible magnetic representations (Shubnikov magnetic space group) $\Gamma_1 (Pbnm)$, $\Gamma_2 (Pbn'm')$, $\Gamma_3 (Pb'nm')$, and $\Gamma_4 (Pb'n'm)$. In Bertraut's notation[24], the three spin components for each representation (Γ_1 to Γ_4) in Cartesian form are

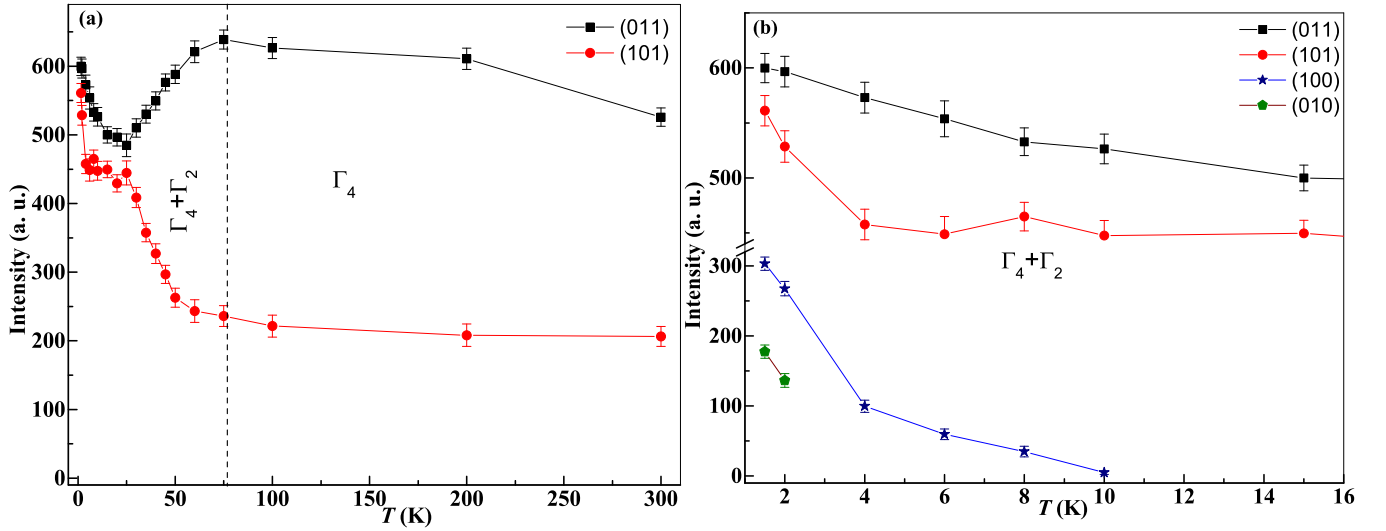


FIG. 6. a) Temperature variation of intensity of various magnetic peaks between 300 and 1.5 K. b) Temperature variation of intensity of various magnetic peaks below 15 K. The development of peaks due to R^{3+} ordering and anomalous rise in the intensity of (101) magnetic peak below 4 K is highlighted.

written as (A_x, G_y, C_z) , (F_x, C_y, G_z) , (C_x, F_y, A_z) and (G_x, C_y, F_z) respectively.

In EDFO, the magnetic structure belongs to Γ_4 representation from 300 K till 75 K which is in agreement with the general behavior of orthoferrites. Based on intensity ratios of peaks, spin reorientation transition starts to occur at 75 K similar to ErFeO_3 . Below 75 K downwards, the magnetic structure is refined as mixed structure given by $\Gamma_4 + \Gamma_2$ representations. The refinements indicate that the spin reorientation in EDFO is of $\Gamma_4 \rightarrow \Gamma_2$ type, which is the usual second order reorientation observed in various orthoferrites. In the temperature range below 60 K, we do not find signature of $\Gamma_4 \rightarrow \Gamma_1$, abrupt transition as

observed in DyFeO_3 . However, the $\Gamma_4 \rightarrow \Gamma_2$ reorientation is not complete even at 1.5 K, the lowest measured temperature.

The rare-earth moments, due to their lower site symmetry can arrange in eight possible representations labelled as Γ_1 to Γ_8 [25]. As shown in Fig. 6b), below 10 K, (100) magnetic peak starts to originate near 26° value of 2θ diffraction angle. From representational analysis, the (100) peak associated with the magnetic ordering of the $\text{Er}^{3+}/\text{Dy}^{3+}$ moments, corresponds to the c_y^R magnetic structure, which belongs the Γ_2 representation. The corresponding magnetic moment is denoted as m_y^R . At

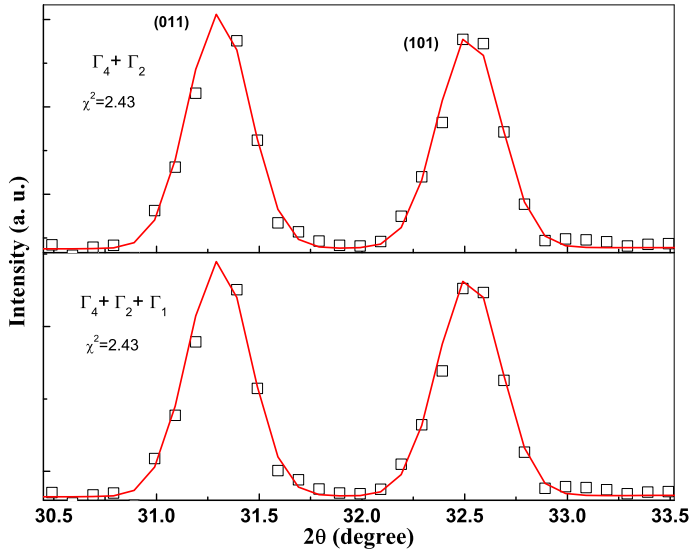


FIG. 7. (color online) (011) and (101) magnetic Bragg peaks showing results of fitting by $\Gamma_4 + \Gamma_2$ (upper panel) and $\Gamma_4 + \Gamma_2 + \Gamma_1$ (lower panel) magnetic structures of the Fe^{3+} spins.

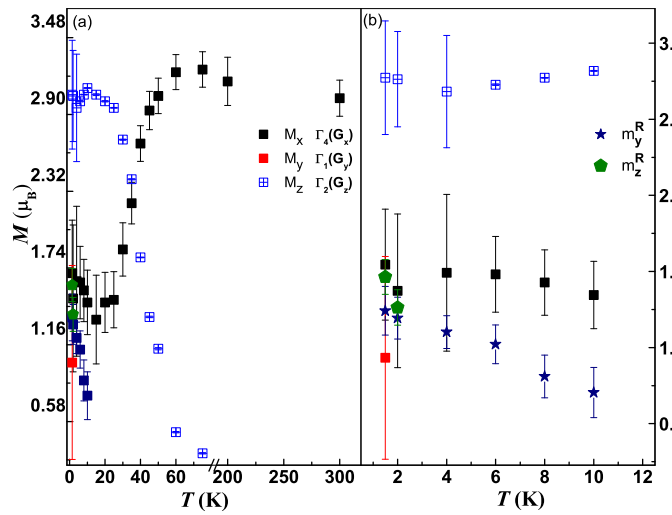


FIG. 8. (color online) a) Temperature variation of magnetic moment of Fe^{3+} and $\text{Er}^{3+}/\text{Dy}^{3+}$ spins from 1.5 K to 300 K for the various magnetic structures. b) The variation of magnetic moments in the temperature range from 10 to 1.5 K. The arrow shows the discontinuity/sudden rise of m_z^R .

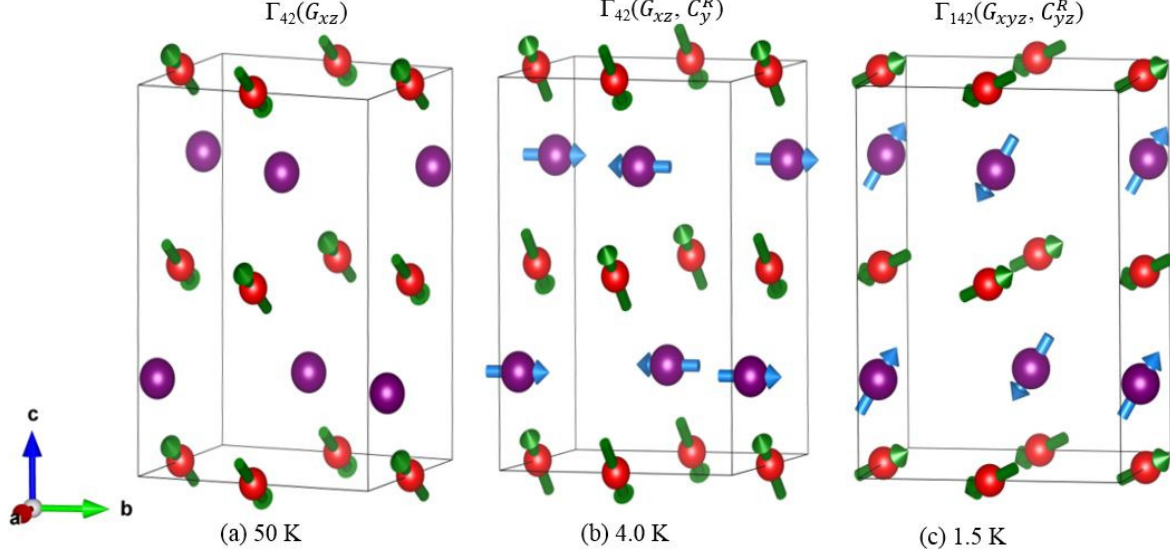


FIG. 9. (color online) Magnetic structure of EDFO at (a) 50 K : G_x, G_z arrangement of Fe^{3+} spins (b) 4 K: (G_x, G_z, c_y^R) (c) 1.5 K: $(G_x, G_y, G_z, c_y^R, c_z^R)$. Red spheres represent Fe atoms, Violet spheres represent Er/Dy atoms

TABLE I. Magnetic structural details of $\text{Er}_{0.5}\text{Dy}_{0.5}\text{FeO}_3$ from present studies and comparison with literature for ErFeO_3 and DyFeO_3 . The “ \rightarrow ” and “ \sim ” denote a complete and incomplete reorientation respectively.

Compound	$T_N > T > T_{SR}$	SR	$T_{SR} > T > T_R$	$T_R > T > 4$ K		T=1.5 K		Reference
	Fe^{3+}	Type	Fe^{3+}	Fe^{3+}	R^{3+}	Fe^{3+}	R^{3+}	
$\text{Er}_{0.5}\text{Dy}_{0.5}\text{FeO}_3$	$G_x F_z$	$\Gamma_4 \sim \Gamma_2$	G_{xz}	G_{xz}	c_y^R	Model1: G_{xz}	$c_y^R c_z^R$	This work
				-		Model2: G_{xyz}	$c_y^R c_z^R$	This work
ErFeO_3	$G_x F_z$	$\Gamma_4 \rightarrow \Gamma_2$	$F_x G_z$	$F_x C_y G_z$	c_z^R			[8, 22, 36–41]
DyFeO_3	$G_x F_z$	$\Gamma_4 \rightarrow \Gamma_1$	G_y	G_{xy}	-	G_{xy}	$g_x^R a_y^R$	[10, 23, 36, 42–45, 49, 50, 53]

2 K, the sudden development of the (010) peak corresponds to the c_z^R arrangement of the $\text{Er}^{3+}/\text{Dy}^{3+}$ moments, which belongs to the Γ_1 representation. The corresponding magnetic moment is denoted as m_z^R . The c_z^R arrangements of Er^{3+} moments were also observed in ErFeO_3 [8, 41]. In ErFeO_3 , the Fe^{3+} show a probable coexistence of Γ_1 and Γ_2 magnetic structures coinciding with c_z^R ordering of the rare-earth[41]. Similarly, at 1.5 K, due to the c_z^R -ordering of the rare earth in EDFO, development of the Γ_1 structure for the Fe^{3+} spins is also expected in addition to combined Γ_{24} structure[8]. The signature of Γ_1 magnetic structure of Fe^{3+} spins can be concurred from the increase in intensity of (101) peak below 4 K as indicated in Fig. 6b). However to confirm this by refinement, the data at 2 and 1.5 K are refined to combinations of Γ_{24} as well as $\Gamma_{24} + \Gamma_1$ structures. At 2 K, the fitting does not converge with inclusion of three phases. However at 1.5 K the goodness of fit is equal in both the cases. In Fig. 7, we show fitting in Γ_{24} (upper panel) and $\Gamma_{24} + \Gamma_1$ (lower panel), highlighting the (011) and (101) peak. Considering all three representations of

$\text{Fe}^{3+}(\Gamma_{24} + \Gamma_1)$, the fitting quality is seems to be slightly better. Moreover, the co-existence of Γ_1 is plausible, since the c_z^R arrangement of $\text{Er}^{3+}/\text{Dy}^{3+}$ moments are symmetry-compatible only with the G_y arrangement of Fe^{3+} spins[8].

The temperature variation of the magnetic moments for the Fe^{3+} and R^{3+} moments for different representations are shown in Fig. 8a). The values of total magnetic moment of Fe^{3+} is nearly $3.2 \mu_B$, which is lower than the theoretical expected value of $5 \mu_B$. Such reduction might be due to effects of covalency, disorder and also the polycrystalline nature of our samples. From 300 K till 75 K we observe a small increase in the magnetic moment (M_x) associated with G_x configuration. With the onset of spin reorientation, there is a decrease in M_x , while correspondingly the M_z shows an increase. Below 20 K both M_x and M_z remain nearly constant with small fluctuations as shown in Fig. 8b). Also, as seen in Fig. 8b), from 10 K till 1.5 K m_y^R shows a gradual increase, while m_z^R shows a sudden development at 2 K.

The m_y^R and m_z^R moments attain values of nearly 1.4 and $1.7 \mu_B$ respectively, resulting in total rare-earth sublattice moment of $2.4 \mu_B$ at 1.5 K. The possible M_y component of the Fe^{3+} moments which only exists at 1.5 K has a much larger error bar as shown in Fig. 8b).

In Table I, we list the magnetic configurations of EDFO at various temperatures. The magnetic configurations of the parent compounds of ErFeO_3 and DyFeO_3 are also listed as reference at the corresponding temperatures. The Fe^{3+} and $\text{Er}^{3+}/\text{Dy}^{3+}$ magnetic structure of EDFO and its variation is closer to ErFeO_3 rather than DyFeO_3 . The magnetic structures of EDFO at 50 K, 4 K and 1.5 K depicting the Fe^{3+} and $\text{Er}^{3+}/\text{Dy}^{3+}$ spins are shown schematically in Figs. 9(a-c).

3. Specific Heat

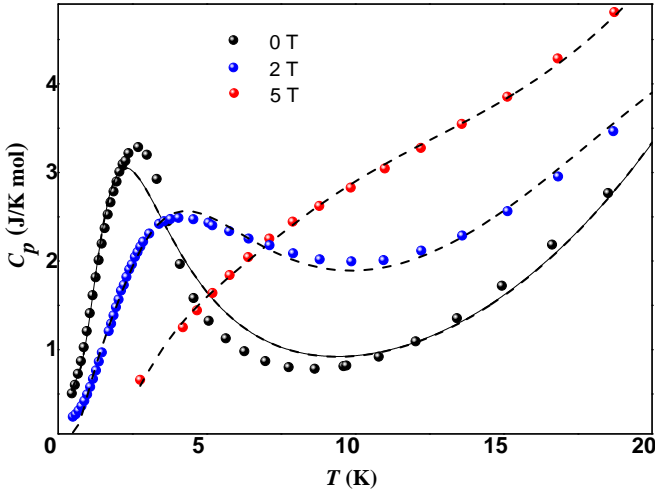


FIG. 10. The low temperature specific heat of EDFO for 0, 2 and 5 T. The dashed and solid lines shows the fitting of specific heat to Schottky and lattice terms

The heat capacity C_p of EDFO for 0, 2 and 5 T are shown in Fig. 10 from 0.4 to 20 K. The zero field heat capacity shows a rise below 8 K with a peak at 2.2 K. The λ -shaped anomaly associated with second order phase transition, seen in DyFeO_3 [48] at 4.2 K is absent in EDFO. Independent magnetic ordering of the R^{3+} ions is absent till 0.4 K which is in agreement with our neutron diffraction results. The feature observed in EDFO is similar to the peak observed in ErFeO_3 due to Schottky effect[77].

In EDFO, the Er^{3+} and Dy^{3+} being odd-electron systems, the ground state of each ion is a Kramer's doublet splitted by molecular, exchange and dipole fields. Thus the low temperature peak in C_p is due to the splitting of the ground state doublet of both the rare-earth ions. To extract information about the splitting of the doublets, the specific heat is fitted in the temperature range 0.4-20 K as a sum of "two-level" Schottky terms corresponding to both the rare-earth ions and the T^3 lattice term as

below,

$$C_p = \frac{1}{2} R \sum_{i=1}^2 w_i \left(\frac{\Delta E_i}{k_B T} \right)^2 \frac{\exp \left[-\frac{\Delta E_i}{k_B T} \right]}{\left(1 + \exp \left[-\frac{\Delta E_i}{k_B T} \right] \right)^2} + B_3 T^3 \quad (1)$$

In Eqn. 1, $\Delta E_1/k_B$ and $\Delta E_2/k_B$ correspond to the doublet splitting in each R^{3+} ion, while B_3 is the lattice term. A single energy splitting is insufficient to simulate the correct magnitude of the peak in C_p . From the fitting, the value $B_3 = 4.04 \times 10^{-4} \text{ J/mole-K}^4$ is obtained which yields a Debye temperature of 457 K for EDFO. At 0 T, we obtain $\Delta E_1/k_B = 1.5 \text{ K}$ and $\Delta E_2/k_B = 5.6 \text{ K}$. These values are well in agreement with the optical spectroscopy studies on both the parent compounds as discussed further.

Optical studies on ErFeO_3 revealed that the splitting of the ground state doublet in the Γ_2 phase is nearly constant from 77 till 5 K with a value of 3.17 cm^{-1} (0.39 meV or 4.52 K)[78]. Similarly, above the Dy^{3+} ordering temperature, the splitting of the ground state doublet in DyFeO_3 is nearly 1.5 cm^{-1} (0.185 meV or 2.14 K) within experimental resolution[79]. The splitting in both cases is attributed to the R^{3+} - Fe^{3+} interactions. Thus, the values of $\Delta E_1/k_B$ and $\Delta E_2/k_B$ in EDFO can be attributed to the doublet splitting in the Dy^{3+} and Er^{3+} ions, respectively. However, due to complex temperature dependence of ΔE , especially in the case of doublet of Er^{3+} ion[80], temperature independent ΔE terms cannot satisfactorily fit the Schottky peak, especially for zero field.

The C_p measured at 2 T, fitting to Eqn. 1 yields, $\Delta E_1 = 5.9 \text{ K}$, while ΔE_2 increases to 26 K. At 5 T, we obtain, $\Delta E_1 = 13.6 \text{ K}$, and $\Delta E_2 = 34 \text{ K}$. Thus effect of magnetic field on the ground state of Er^{3+} is more drastic, indicating greater polarizability due to external fields. The values of ΔE for both ions though obtained directly from Zeeman effect studies on both the parent compounds[78, 79, 81].

IV. DFT CALCULATIONS

The magnetic structure of EDFO is also explored using density functional theory. In the $Pbnm$ structure, the Er and Dy atoms occupy the $8c$ sites in a random fashion. For computational purposes, we have considered two regular arrangements of Er and Dy atoms, viz. the (111) and (001) arrangements[75]. In the (111) arrangement, the Er and Dy atoms are placed adjacent to each other. Thus each Er atom has six Dy atoms as nearest neighbours and vice versa. In the (001) arrangement, Er and Dy atomic planes are alternately stacked along the c axis[75].

For both the cationic arrangements, structural relaxation of the orthorhombic unit cell have been performed using the experimental structural parameters obtained for 300 K and 1.5 K. The structure was relaxed considering G-type magnetic ordering of the Fe^{3+} magnetic mo-

TABLE II. Relative energies (in meV) for two main antiferromagnetic orders of R^{3+} ion within GGA+ U ($U=8.5$ eV and $J=0.5$ eV) for the two Er/Dy arrangements.

Magnetic structure	alternate (111)	layered (001)
C-type	0	0
G-type	+9.76	+16.46

ments. The electronic self-consistent calculations were performed to obtain the magnetic structure and spin-resolved density of states (DOS) of EDFO, for which the Hubbard U on Fe and Er/Dy was incorporated. The Hubbard parameters $U=8.5$ eV, $J=0.5$ eV for Er and Dy; $U=5.0$ eV and $J=1$ eV for Fe are used. The iterations were performed till an energy difference of 10^{-6} eV was achieved. Energetically, it is found that the (001) arrangement has lower energy as compared to (111) arrangement.

In the case of Fe^{3+} sublattice, the lowest energy corresponds to G-type magnetic ordering which is common in all orthoferrites[82]. In probing the rare-earth ordering, we have considered two possible arrangements of the Er^{3+}/Dy^{3+} moments, a) C-type and b) G-type. The Fe^{3+} ordering was fixed as G-type in these calculations. For both cationic arrangements of Er and Dy atoms, C-type magnetic structure emerges with lower energy, consistent with the neutron diffraction results. The relative energies are listed in Table II. The energy difference between both magnetic structures is greater for the layered arrangement as compared to the alternate arrangement of Er and Dy. The magnetic moment of Fe^{3+} obtained from DFT is $4.2 \mu_B$, which is smaller than the free ion value of $5 \mu_B$ and larger than the experimentally observed value. The reduction can be attributed to effects of hybridization with the O $2p$ band. Moment values of Er and Dy are $3 \mu_B$ and $5 \mu_B$ respectively, since we do not consider the effects of spin-orbit coupling in our calculations.

Fig. 11a) and b) show the spin resolved partial density of states of EDFO for (111) and (001) arrangements. In both arrangements, a band gap of ~ 2.2 eV is obtained. Just below the Fermi energy, the spectral character of DOS is mainly the combination of strongly hybridized Fe $3d$ and O $2p$ states. In both the arrangements, the behavior of Fe $3d$ bands appear similar.

The $4f$ states of Er and Dy show a different behavior in both the arrangements. For (111) arrangement, below the Fermi energy, Er $4f$ (\uparrow and \downarrow) DOS show a series of sharp spectral features in the range -5 to -7 eV. The Dy states occur much below Fermi level (-7 to -8 eV), highly confined and does not overlap with the states of any other element.

For (001) arrangement, a strong hybridization between Er $4f$ (\uparrow and \downarrow) and Fe $3d/O$ $2p$ states occur around -5 eV below which there is a gap in the range -6 to -7 eV, the Er $4f$ \uparrow states are strongly hybridized compared to

the \downarrow states. The Dy $4f$ states occur between -7 to -8 eV without any signature of overlap. Above the Fermi level, $4f$ bands of both Er and Dy are more discrete and do not show any overlap with the Fe and O DOS.

The strengths of the magnetic exchange interactions between $Er^{3+}-Er^{3+}$, $Dy^{3+}-Dy^{3+}$ and $Er^{3+}-Dy^{3+}$ have been determined from our density functional theory calculations. Additionally, the strengths of $Er^{3+}/Dy^{3+}-Fe^{3+}$ exchange interactions are also determined. The differences in energies of ferromagnetic and anti-ferromagnetic arrangements are mapped to the Heisenberg Hamiltonian[82, 83]. The calculations were performed on “artificial unit cells using the experimental structure of 1.5 K, in which except for the selected Fe or Er/Dy atoms, the rest of magnetic atoms are replaced by non-magnetic atoms. Thus the Fe atom is replaced by Al, while both Er and Dy are replaced by La atoms, since La^{3+} ion is non-magnetic[82].

From the calculations, it is found that the $Dy^{3+}-Fe^{3+}$ interaction is the weakest, with a value of 0.019 meV, which is smaller than the single ion anisotropy of Dy^{3+} ion. The $Er^{3+}-Fe^{3+}$ interaction, with a much higher value of 2.88 meV thus plays important role in the $\Gamma_4 \rightarrow \Gamma_2$ reorientation. Among the interaction strengths between the rare-earths, the $Dy^{3+}-Dy^{3+}$ exchange interaction is found to be 1.21 meV. This is consistent with the fact that the interaction between the Dy^{3+} ions which include the exchange and dipolar interactions result in long range ordering at 4.5 K in $DyFeO_3$. The $Er^{3+}-Er^{3+}$ interaction is also found to be small with a value of -0.037 meV. This is consistent with the fact though the Er^{3+} moments can be polarized by the molecular field of Fe, suppressing the independent ordering of Er^{3+} moments in $ErFeO_3$. The $Er^{3+}-Dy^{3+}$ exchange interactions has an appreciable value of 1.38 meV, which helps in the establishment of the long-range ordering by polarization of the Er/Dy sublattice below 10 K.

V. DISCUSSION

A. $\Gamma_4 \rightarrow \Gamma_2$ “incomplete” reorientation of Fe^{3+} spins

In the Γ_4 phase below the T_{N1} , due to the F_z component of Fe^{3+} spins, an effective molecular field along the z axis develops. Such effective field induces a net polarization on the R^{3+} moments, which by symmetry, should align as f_z^R .

The $Er^{3+}-Fe^{3+}$ interactions are much greater than the $Dy^{3+}-Fe^{3+}$ interactions as seen in our first principles calculations and optical studies[78, 79]. The anisotropic and anti-symmetric exchange interactions part of Er^{3+} and Fe^{3+} exchange interactions, cause rotation of the Fe^{3+} spins below 75 K, resulting in the $\Gamma_4 \rightarrow \Gamma_2$ reorientation near 75 K. This behavior is identical to reorientation in $ErFeO_3$ [41]. According to the effective field model by Yamaguchi *et al*[47], the anisotropic-symmetric exchange interactions between Fe^{3+} and R^{3+} is primarily respon-

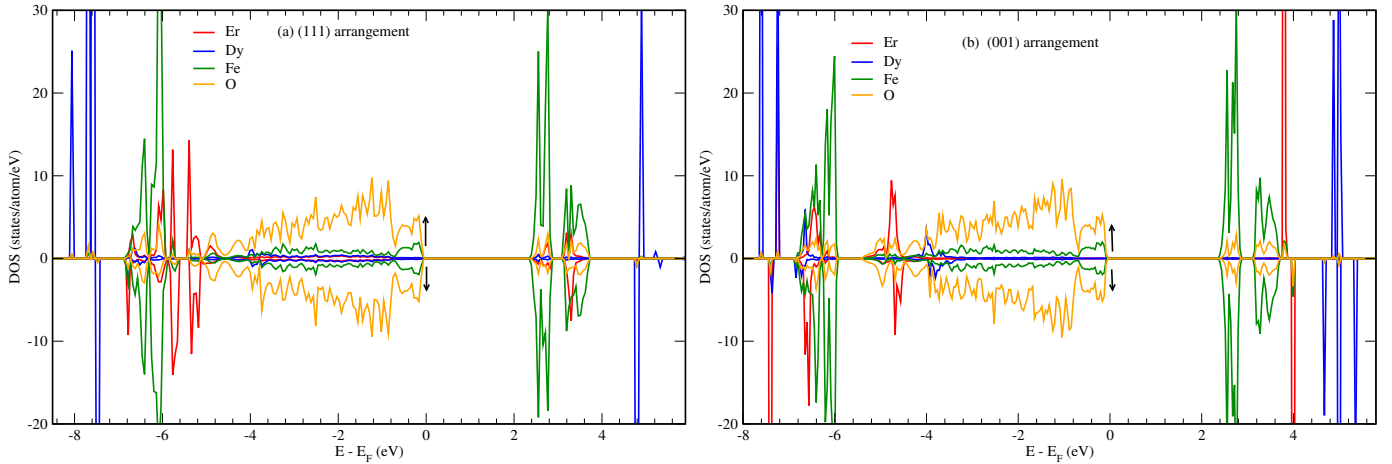


FIG. 11. Spin resolved density of states(DOS) of EDFO for the (a) alternate(111) (b) layered(001) arrangements of Er and Dy corresponding to the C-type ordering of rare-earth and G-type ordering of Fe moments. The \uparrow and \downarrow correspond to spin up and down regions respectively.

sible for such a gradual spin-reorientation.

During reorientation, the spontaneous weak ferromagnetic component of Fe^{3+} moments changes from F_z to F_x . Due to two dissimilar rare-earth ions, a local variation in exchange field develops in the system. The Dy^{3+} ions do not affect the spin reorientation much, since the negligible Dy^{3+} - Fe^{3+} interaction does not play a major role. Thus, instead of reorientation occurring in a short interval of 10 K as in ErFeO_3 [41], a very gradual reorientation takes place in EDFO. This results in co-existence of $\Gamma_4(G_x, C_y, F_z)$ and $\Gamma_2(F_x, C_y, G_z)$ in the entire temperature range below 75 K, wherein F_z and F_x play role similar to the external applied field.

The external field along various crystal axes, cause spin reorientations in both the parent compounds. However, compared to ErFeO_3 [73], the effect of field is more drastic in DyFeO_3 at smaller fields. For field along a direction, above a critical field (of nearly 1-2 T), a $\Gamma_1 \rightarrow \Gamma_4$ transition is induced. A relatively small field along c -direction and b -direction, $\Gamma_1 \rightarrow \Gamma_2$ reorientation is induced in DyFeO_3 [43]. The effective molecular fields along the a, b and c -directions eventually suppress the Morin transition in EDFO. At 50 K a co-existence of both the magnetic structures exists as shown in Figs. 9a, which persists till 1.5 K. We also explored the possibility of an additional magnetic phase Γ_1 in addition of the Γ_{24} at 1.5 K. Hence, the spin reorientation in EDFO can be considered to be an “incomplete reorientation”.

B. Polarization of rare-earth moments

1. Development of c_y^R arrangement of R^{3+} moments

Just as the predominant Er^{3+} - Fe^{3+} interactions cause the $\Gamma_4 \rightarrow \Gamma_2$ reorientation, this also results in the polarization of the R^3 moments in the (f_x^R, c_y^R) configuration. The po-

larization of Er^{3+} moments are lot easier as compared to the Dy^{3+} moments. Though the preferred arrangement of Dy^{3+} moments is (g_x^R, a_y^R) , this is actually the spin-flopped configuration of (f_x^R, c_y^R) with the energy difference smaller than the single ion anisotropy of Dy^{3+} [47]. Thus the effective field along the x axis can also partially polarize the Dy^{3+} moments along with the Er^{3+} moments. Hence, at 4 K, Fe^{3+} spins are in Γ_{42} configuration, the R^{3+} moments are in c_y^R -configuration(Fig. 9b).

2. Development of c_z^R arrangement of R^{3+} moments

At 2 K, a sudden appearance of the c_z^R magnetic Bragg peaks occurs. As shown in Fig. 8b), the magnetic moment (m_z^R) shows a sudden rise. The mechanism behind the sudden appearance of c_z^R and abrupt reorientation $G_x \rightarrow G_y$, which is characteristic feature of ErFeO_3 , is more complex to understand. In Fig. 9c), we show the coexistence of c_y^R and c_z^R along with Fe^{3+} spins having (G_x, G_y, G_z) at 1.5 K.

C. Analysis of the rare-earth ordering

The ground state of Dy^{3+} and of Er^{3+} ions viz. ${}^6H_{15/2}$ and ${}^4I_{15/2}$ respectively, are split by the monoclinic crystal field ($C_s(m)$) into eight Kramer’s doublets[51, 81]. Inelastic neutron studies reveal that the splitting between the ground state and first excited doublet of Er^{3+} is around 5.5 meV, while in the case of Dy^{3+} a separation of nearly 6.8 meV is observed. Below 50 K, only the lowest doublet is populated in both ions. Hence, the Er^{3+} and Dy^{3+} ions are described as “effective spin” $S_R=1/2$ (R :rare-earth) systems which are two-fold degenerate. The degeneracies of ground state of both ions are Zeeman split by an energy ΔE due to external field as well as internal molecu-

lar fields, \vec{H}_{eff} due to R^{3+} - Fe^{3+} , R^{3+} - R^{3+} , exchange and dipolar interactions. The coupling of the Er^{3+} and Dy^{3+} ‘spins’ to the effective fields occur via the anisotropic ‘ \mathbf{g} ’ tensor[78, 79].

Mean field studies pertaining to rare-earth magnetism in $R\text{CrO}_3$ ($R=\text{Nd}, \text{Er}$), show that temperature evolution of magnetic moment of R^{3+} and ΔE are related in a self-consistent manner. The sub-lattice magnetization of R^{3+} is defined as $m^R=1/2g_y\mu_B N\langle S_R \rangle$; where the thermal average of the R^{3+} ‘spin’ is related to the doublet splitting as, $\langle S_R \rangle=B_S(\Delta E/k_B T)$. Here, $B_S(x)$ is the Brillouin function which for $S_R=1/2$ becomes $\tanh(x)$ [84].

Optical spectroscopy and mean field analysis on NdCrO_3 and ErCrO_3 show that below the T_{N1} , ΔE is proportional to temperature dependent sublattice magnetization of Cr^{3+} spins $\langle S \rangle/S$ ($S=3/2$ for Cr^{3+}). However, below the spin reorientation temperature (T_{SR}), when the R^{3+} - R^{3+} interactions become non-negligible, ΔE is proportional to sum of a) sublattice magnetization of Cr^{3+} spins and b) $\tanh(\Delta E(\vec{H}, T)/2k_B T)$ [80, 84].

In EDFO, the situation is more complex, since the temperature dependence of ΔE , is different for the Er^{3+} and Dy^{3+} ions. Thus in EDFO, the variation in m_y^R can be attributed to sum of the three terms, a) Fe^{3+} sublattice magnetization, b) $\tanh(\Delta E_{\text{Er}}(\vec{H}, T)/2k_B T)$ and c) $\tanh(\Delta E_{\text{Dy}}(\vec{H}, T)/2k_B T)$. In EDFO, even above 75 K, the Fe^{3+} spins have attained their maximum value. In the range 1.5-10 K the net sub-lattice magnetic moment of Fe^{3+} is nearly constant. Thus, the temperature dependence of ΔE for both R^{3+} ions on the Fe^{3+} sublattice magnetization is less pronounced. The eventual rise of m_y^R below 10 K can be attributed to the interaction between the R^{3+} ions. In view of the negligible Er^{3+} - Er^{3+} exchange interactions, the increase in m_y^R can be attributed to the Dy^{3+} - Dy^{3+} exchange and dipole interactions. Though optical spectroscopy studies on DyFeO_3 and DyAlO_3 suggest only a stronger dipole interaction, our first principles calculations suggest a strong exchange interaction can also exist between the Dy^{3+} moments. Additionally, the Er^{3+} - Dy^{3+} exchange interactions which are comparable to the Dy^{3+} - Dy^{3+} interactions, also contribute to the c_y^R ordering.

At 2 K, due to development of c_z^R -ordering, the total R^{3+} sub-lattice magnetic moment shows sudden increase. Similar behavior is observed in ErFeO_3 , in which below 5 K the Er^{3+} moments order as c_z^R along with increase in ΔE , which attains a maximum value of 6.5 cm^{-1} (0.8 meV or 10 K)[78]. In orthochromate ErCrO_3 , a discontinuity in ΔE occurs at T_{SR} [80] accompanied by the c_z^R ordering of Er^{3+} moments. The Er^{3+} - Er^{3+} dipole interaction which causes the c_z^R ordering, is maximum between Er^{3+} moments along the c direction[80, 81].

Even though the dipole interactions result in magnetic ordering of the R^{3+} ions at the lowest temperature, the direction of the moments are decided by the anisotropic \mathbf{g} tensor. From optical spectra of ErFeO_3 , it was observed that $g_{xx}(\text{min})=1.2$, $g_{yy}(\text{max})=4.5$ and g_{zz}

($z||c$ -axis)= 5.6 in a - b plane[81]. Thus, a slightly larger anisotropy along the z axis facilitates the c_z^R ordering of the Er^{3+} moments below 5 K. In Dy^{3+} , $g_{xy}(\text{min})=3.2$, $g_{xy}(\text{max})=18.4$, $g_{zz}=2.0$, due to which the Dy^{3+} moments have a strong Ising character with moments in direction of $g_{xy}(\text{max})$ [51] which is also clear from the long range antiferromagnetic ordering of Dy^{3+} moments with $\Gamma_5(g_x^R, a_y^R)$ configuration in DyFeO_3 , DyAlO_3 , DyScO_3 . Thus the c_z^R is completely opposed by the the a - b plane anisotropy, even though optical studies on DyAlO_3 reveal that Dy^{3+} - Dy^{3+} dipole interaction has maximum strength along the c direction [85]. Estimate of the dipolar energy in DyScO_3 for various magnetic configurations in the a - b plane reveal that for the experimental (g_x^R, a_y^R) configuration, the lowest dipolar energy (-3.61 K) is achieved which is also close to the T_{N2} , while the (f_x^R, c_y^R) has the highest energy (+2.44 K) at zero field[53].

In a similar manner, estimate of the ground state energy of the rare-earth in the context of dipolar energy is carried out in EDFO. The magnitude of magnetic moments are fixed according to the experimentally obtained values. The dipolar energy is calculated for Er and Dy arranged alternately for a radii of nearly 6 Å containing eighteen atoms. For the four magnetic arrangements, $c_z^R, c_y^R, (c_y^R, c_z^R)$ and (g_x^R, a_y^R) , the energies obtained are -0.158 K, +0.092 K, -0.08 K and -0.138 K respectively. Thus the c_z^R ordering is most favoured by the Er^{3+} - Dy^{3+} dipolar interaction while c_y^R ordering is least favoured. However, the character of \mathbf{g} tensor of Dy^{3+} tends to suppress the c_z^R ordering to lower temperature, due to which the peaks appear only at 2 K with a lower magnetic moment than observed in ErFeO_3 .

D. Symmetry of ground state

Finally, we discuss the symmetry aspects of the magnetic structure of EDFO at 1.5 K. Based on the representation analysis, the resultant magnetic structure can be written as $\Gamma_4+\Gamma_2+\Gamma_1$. To simplify things, we consider the net magnetic structure at 1.5 K as combinations of Γ_{24}, Γ_{14} and Γ_{12} . The Γ_{12} and Γ_{14} belong to the point group $C_{2h}(C_{2h})(m)$, while the Γ_{24} belongs to the point group $C_{2h}(C_i)(m')$ [47]. The Γ_{14} and Γ_{12} are invariant under the symmetry operations $(E, \tilde{C}_{2x}, i, i\tilde{C}_{2x})$ and $(E, \tilde{C}_{2z}, i, i\tilde{C}_{2z})$, respectively. On the other hand, the Γ_{24} is invariant under $(E, i, R\tilde{C}_{2y}, iR\tilde{C}_{2y})$. Here i corresponds to the inversion symmetry operation and R corresponds to time reversal symmetry operator. In the case of Γ_{24} , there occurs an effective field, which is absent in the case of Γ_1 . Considering the coexistence of three phases, the only symmetry elements remaining are (E, i) . The presence of inversion symmetry rules out possibility of a spontaneous ferroelectric polarization. Moreover, reduction in the structural symmetry due to the simultaneous presence of c_y^R and c_z^R does not occur, unlike speculated

by Deng *et al.*[8]. The absence of any ferroelectric polarization or magnetodielectric effect is also confirmed by temperature dependent dielectric studies in presence of the magnetic field (data is not shown).

However the coexistence c_y^R and c_z^R structures coincides with a negative volume expansion occurs below 10 K as shown in Fig. 2(e). Though this suggests a magneto-volume effect, the detailed analyses are beyond the scope of this paper.

E. Conclusion

In conclusion, we have investigated magnetic behavior of polycrystalline EDFO using various experimental techniques like bulk magnetization, neutron powder diffraction and specific heat, while the observed properties were correlated with theoretical estimations from density functional theory. At 300 K, magnetic structure belongs to Γ_4 configuration. The 50% substitution of Er^{3+} and Dy^{3+} results in a complex spin reorientation of EDFO. The gradual $\Gamma_4 \rightarrow \Gamma_2$ reorientation of the Fe^{3+} spins begin below 75 K. However, the reorientation remains incomplete even at 10 K and continue to coexist at lower temperatures. The ordering of rare-earth due to its polarization starts below 10 K resulting in c_y^R peak in the Γ_2 representation. At 2 K, the sudden development of the c_z^R magnetic peak occurs, which can initiate the sudden ro-

tation of the Fe^{3+} spins in the y direction. The specific heat shows a Schottky peak of relatively larger intensity, indicating the absence of second order phase transition. The strengths of exchange interactions estimated from density functional theory calculations suggest that the Er^{3+} - Fe^{3+} , Er^{3+} - Dy^{3+} and Dy^{3+} - Dy^{3+} exchange interactions are of comparable strength, while the Er^{3+} - Er^{3+} and Dy^{3+} - Fe^{3+} interactions are the weakest. The C-type ordering of rare-earth magnetic moments is consistent with experimental data. The development of c_z^R can be attributed to the Er^{3+} - Er^{3+} dipole interactions, while the strong anisotropy of Dy^{3+} ions tend to suppress this transition to lower temperature.

F. Acknowledgment

This work was supported by the UGC-DAE Consortium for Scientific Research (CSR) and Science and Engineering Research Board (SERB) through CRS-M-228, ECR/2015/000136, respectively. We acknowledge the support from IIT Roorkee through SMILE-13 grant. AS and SR acknowledge MHRD for research fellowships. CMNK and WT acknowledge support from the Polish National Agency for Academic Exchange under the Polish Returns 2019 programme, grant PPN/PPO/2019/1/00014"

-
- [1] J. Guo, L. Cheng, Z. Ren, W. Zhang, X. Lin, Z. Jin, S. Cao, Z. Sheng, and G. Ma, *Journal of Physics: Condensed Matter* **32**, 185401 (2020).
- [2] R. V. Mikhaylovskiy, T. J. Huisman, A. I. Popov, A. K. Zvezdin, T. Rasing, R. V. Pisarev, and A. V. Kimel, *Phys. Rev. B* **92**, 094437 (2015).
- [3] R. V. Mikhaylovskiy, E. Hendry, A. Secchi, J. H. Mentink, M. Eckstein, A. Wu, R. V. Pisarev, V. V. Kruglyak, M. I. Katsnelson, T. Rasing, and A. V. Kimel, *Nature Communications* **6**, 8190 (2015).
- [4] R. V. Mikhaylovskiy, E. Hendry, V. V. Kruglyak, R. V. Pisarev, T. Rasing, and A. V. Kimel, *Phys. Rev. B* **90**, 184405 (2014).
- [5] K. Yamaguchi, T. Kurihara, Y. Minami, M. Nakajima, and T. Suemoto, *Phys. Rev. Lett.* **110**, 137204 (2013).
- [6] S. Ding, M. Xue, Z. Liang, Z. Liu, R. Li, S. Cao, Y. Sun, J. Zhao, W. Yang, and J. Yang, *Journal of Physics: Condensed Matter* **31**, 435801 (2019).
- [7] A. V. Kimel, A. Kirilyuk, A. Tsvetkov, R. V. Pisarev, and T. Rasing, *Nature* **429**, 850 (2004).
- [8] G. Deng, P. Guo, W. Ren, S. Cao, H. E. Maynard-Casely, M. Avdeev, and G. J. McIntyre, *Journal of Applied Physics* **117**, 164105 (2015).
- [9] Y. Du, Z. X. Cheng, X. L. Wang, and S. X. Dou, *Journal of Applied Physics* **107**, 09D908 (2010).
- [10] Y. Tokunaga, S. Iguchi, T. Arima, and Y. Tokura, *Physical Review Letters* **101**, 097205 (2008).
- [11] H. Yokota, T. Nozue, S. Nakamura, H. Hojo, M. Fukunaga, P.-E. Janolin, J.-M. Kiat, and A. Fuwa, *Phys. Rev. B* **92**, 054101 (2015).
- [12] A. Singh, S. Rajput, B. Padmanabhan, K. Kedarsh, M. Anas, T. Maitra, and V. K. Malik, *Journal of Physics: Condensed Matter* **31**, 355802 (2019).
- [13] Y. J. Ke, X. Q. Zhang, Y. Ma, and Z. H. Cheng, *Scientific Reports* **6**, 19775 (2016).
- [14] T. Chakraborty, R. Yadav, S. Elizabeth, and H. L. Bhat, *Physical Chemistry Chemical Physics* **18**, 5316 (2016).
- [15] K. Knížek, J. Hejtmanek, Z. Jiráček, P. Tomeš, P. Henry, and A. Gilles, *Physical Review B* **79**, 134103 (2009).
- [16] W. Sławiński, R. Przeniosło, I. Sosnowska, and E. Suard, *Journal of Physics: Condensed Matter* **17**, 4605 (2005).
- [17] N. L. Ross, J. Zhao, J. B. Burt, and T. D. Chaplin, *Journal of Physics: Condensed Matter* **16**, 5721 (2004).
- [18] A. M. Glazer, *Acta Crystallographica Section B* **28**, 3384 (1972).
- [19] P. M. Woodward, *Acta Crystallographica Section B* **53**, 32 (1997).
- [20] P. M. Woodward, *Acta Crystallographica Section B* **53**, 44 (1997).
- [21] R. J. P. Marezio M. and D. P. D., *Acta Crystallogr. B* **26**, 2008 (1970).
- [22] W. C. Koehler, E. O. Wollan, and M. K. Wilkinson, *Phys. Rev.* **118**, 58 (1960).
- [23] R. L. White, *Journal of Applied Physics* **40**, 1061 (1969).
- [24] E. F. Bertaut, *Magnetism III*, edited by G. T. Rado and H. Suhl (Academic Press, New York, 1963).
- [25] T. Yamaguchi, *J. Phys. Chem. Solids*. **35**, 479 (1974).

- [26] J. Bartolomé, E. Palacios, M. D. Kuz'min, F. Bartolomé, I. Sosnowska, R. Przeniosło, R. Sonntag, and M. M. Lukina, *Physical Review B* **55**, 11432 (1997).
- [27] H. Pinto and H. Shaked, *Solid State Communication* **10**, 663 (1972).
- [28] I. Sosnowsk, E. Steichelea, and A. Hewatc, *Physica B+C* **136**, 394 (1986).
- [29] R. Przeniosło, I. Sosnowska, P. Fischer, W. Marti, F. Bartolomé, J. Bartolomé, E. Palacios, and R. Sonntag, *Journal of Magnetism and Magnetic Materials* **160**, 370 (1996).
- [30] S. Yuan, Y. Wang, M. Shao, F. Chang, B. Kang, Y. Isikawa, and S. Cao, *Journal of applied physics* **109**, 07E141 (2011).
- [31] G. Song, J. Jiang, B. Kang, J. Zhang, Z. Cheng, G. Ma, and S. Cao, *Solid State Communications* **211**, 47 (2015).
- [32] J. Jiang, G. Song, D. Wang, Z. Jin, Z. Tian, X. Lin, J. Han, G. Ma, S. Cao, and Z. Cheng, *Journal of Physics: Condensed Matter* **28**, 116002 (2016).
- [33] L. Chen, T. Li, S. Cao, S. Yuan, F. Hong, and J. Zhang, *Journal of applied physics* **111**, 103905 (2012).
- [34] R. Przeniosło, I. Sosnowska, and P. Fischer, *Journal of Magnetism and Magnetic Materials* **140-144**, 2153 (1995).
- [35] M. D. F. Bartolomé, M.D. Kuz'min, J. Bartolomé, J. Blasco, J. Garcia, and F. Sapifia, *Solid State Communications* **91**, 177 (1994).
- [36] R. M. Bozorth, V. Kramer, and J. P. Remeika, *Phys. Rev. Lett.* **1**, 3 (1958).
- [37] R. W. Grant and S. Geller, *Solid State Communications* **7**, 1291 (1969).
- [38] Y. B. Bazaliy, L. T. Tsymba, G. N. Kakazei, A. I. Izotov, and P. E. Wige, *Physical Review B* **69**, 104429 (2004).
- [39] H. Pinto, G. Shachar, H. Shaked, and S. Shtrikman, *Phys. Rev. B* **3**, 3861 (1971).
- [40] L. T. Tsymbal, Y. B. Bazaliy, V. N. Derkachenko, V. I. Kamenevand, G. N. Kakazei, F. J. Palomares, and P. E. Wigen, *Journal of applied physics* **101**, 123919 (2007).
- [41] G. Gorodetsky, R. M. Hornreich, I. Yaeger, H. Pinto, G. Shachar, and H. Shaked, *Phys. Rev. B* **8**, 3398 (1973).
- [42] G. Gorodetsky, B. Sharon, and S. Shtrikman, *Journal of Applied Physics* **39**, 1371 (1968).
- [43] L. A. Prelorendjo, C. E. Johnson, M. F. Thomas, and B. M. Wanklyn, *Journal of Physics C: Solid State Physics* **13**, 2567 (1980).
- [44] Z. Y. Zhao, X. Zhao, H. D. Zhou, F. B. Zhang, Q. J. Li, C. Fan, X. F. Sun, and X. G. Li, *Physical Review B* **89**, 224205 (2014).
- [45] J. Wang, J. Liu, J. Sheng, W. Luo, F. Ye, Z. Zhao, X. Sun, S. A. Danilkin, G. Deng, and W. Bao, *Physical Review B* **93**, 140403 (2016).
- [46] F. J. Morin, *Phys. Rev.* **78**, 819 (1950).
- [47] T. Yamaguchi, *Physical review B* **8**, 5187 (1973).
- [48] A. Berton and B. Sharon, *Journal of Applied Physics* **39**, 1367 (1968).
- [49] I. Nowik and H. Williams, *Physics Letters* **20**, 154 (1966).
- [50] K. P. Belov, A. M. Kadomtseva, L. M. Ledneva, T. L. Ovchinnikova, Y. G. Panomarev, and V. A. Timofeeva, *Soviet Physics-Solid State* **9**, 2190 (1968).
- [51] L. M. Holmes, L. G. V. Uitert, R. R. Hecker, and G. W. Hull, *Physical Review B* **5**, 138 (1972).
- [52] I. B. Krynetskii and V. M. Matveev, *Phys. Solid State* **39**, 584 (1997).
- [53] L. S. Wu, S. E. Nikitin, M. Frontzek, A. I. Kolesnikov, G. Ehlers, M. D. Lumsden, K. A. Shaykhtudinov, E. J. Guo, A. T. Savici, Z. Gai, A. S. Sefat, and A. Podlesnyak, *Physical Review B* **96**, 144407 (2017).
- [54] A. K. Zvezdin and A. A. Mukhin, *JETP Letters* **88**, 505 (2009).
- [55] B. Rajeswaran, D. Sanyal, C. Mahuya, Y. Sundarayya, A. Sundaresan, and C. N. R. Rao, *Euro Physics Letters* **101**, 17001 (2013).
- [56] S. Ankita, A. Jain, R. Avijeet, B. Padmanabhan, Y. Ruchika, N. Vivian, H. Sajid, S. M. Yusuf, T. Maitra, and V. K. Malik, *Physical review B* **96**, 144420 (2017).
- [57] Y. Tokunaga, Y. Taguchi, T. Arima, and Y. Tokura, *Phys. Rev. Lett.* **112**, 037203 (2014).
- [58] M. Mihalik, M. Mihalik, M. Fitta, M. Bałanda, M. Vavra, S. Gabáni, M. Zentková, and J. Briancin, *Journal of Magnetism and Magnetic Materials* **345**, 125 (2013).
- [59] T. Chakraborty and S. Elizabeth, *Journal of Magnetism and Magnetic Materials* **462**, 78 (2018).
- [60] H. Wu, S. Cao, M. Liu, Y. Cao, B. Kang, J. Zhang, and W. Ren, *Physical review B* **90**, 144415 (2014).
- [61] J. Lazurova, M. Mihalik, M. M. jr., M. Vavra1, M. Zentkova1, J. Briancin, M. Perovic, V. Kusigerski, O. Schneeweiss, P. Roupцова, K. V. Kamenev, M. Misek, and Z. Jaglicic, *Journal of Physics: Conference Series* **592**, 012117 (2015).
- [62] T. Chakraborty, R. Yadav, S. Elizabeth, and H. L. Bhat, *Physical Chemistry and Chemical Physics* **18**, 536 (2016).
- [63] H. S. Nair, T. Chatterji, C. M. N. Kumar, T. Hansen, H. Nhalil, S. Elizabeth, and A. M. Strydom, *Journal of Applied Physics* **119**, 053901 (2016).
- [64] T. Chakraborty and S. Elizabeth, *Journal of Magnetism and Magnetic Materials* **462**, 78 (2018).
- [65] H. Rietveld, *Journal of Applied Crystallography* **2**, 65 (1969).
- [66] J. Rodriguez-Carvajal, in *satellite meeting on powder diffraction of the XV congress of the IUCr*, Vol. 127 (Toulouse, France:[sn], 1990).
- [67] E. Hovestreydt, M. Aroyo, S. Sattler, and H. Wondratschek, *Journal of Applied Crystallography* **25**, 544 (1992).
- [68] G. Kresse and J. Furthmüller, *Physical review B* **54**, 11169 (1996).
- [69] J. P. Perdew, K. Burke, and M. Ernzerhof, *Physical Review Letters* **77**, 3865 (1996).
- [70] V. I. Anisimov, I. V. Solovyev, M. A. Korotin, M. T. Czyzyk, and G. A. Sawatzky, *Physical Review B* **48**, 16929 (1993).
- [71] C. M. N. Kumar, Y. Xiao, P. Lunkenheimer, A. Loidl, and M. Ohl, *Physical Review B* **91**, 235149 (2015).
- [72] H. Shen, Z. Cheng, F. Hong, X. Jiayue, S. Yuan, S. Cao, and X. Wang, *Applied Physics Letters* **103**, 192404 (2013).
- [73] X. X. Zhang, Z. C. Xia, Y. J. Ke, X. Q. Zhang, Z. H. Cheng, Z. W. Ouyang, J. F. Wang, S. Huang, F. Yang, Y. J. Song, G. L. Xiao, H. Deng, and D. Q. Jiang, *Physical review B* **100**, 054418 (2019).
- [74] A. Epstein and H. Shaked, *Physical Letters* **29A**, 659 (1969).
- [75] A. Singh, S. Rajput, P. Balasubramanian, M. Anas, F. Damay, C. M. N. Kumar, G. Eguchi, A. Jain, S. M. Yusuf, T. Maitra, and V. K. Malik, *Phys. Rev. B* **102**, 144432 (2020).

- [76] E. F. Bertaut, *Acta Crystallographica* **A24**, 217 (1967).
- [77] K. Saito, Y. Yamamura, J. Mayerb, H. Kobayashi, Y. Miyazakia, J. Ensling, P. Gütlich, B. Leśniewska, and M. Sorai, *Journal of Magnetism and Magnetic Materials* **225**, 381 (2001).
- [78] R. Faulhaber, E. Hüfner, E. Orlich, and H. Schuchert, *Zeitschrift für Physik* **204**, 101 (1967).
- [79] H. Schuchert and R. Hüfner, E. Faulhaber, *Zeitschrift für Physik* **220**, 273 (1969).
- [80] A. Hasson, R. M. Hornreich, Y. Komett, B. M. Wanklyn, and I. Yaeger, *Physical Review B* **12**, 5051 (1975).
- [81] D. L. Wood, L. M. Holmes, and J. P. Remeika, *Physical review B* **185**, 689 (1969).
- [82] C. Weingart, N. Spaldin, and E. Bousquet, *Physical Review B* **86**, 094413 (2012).
- [83] J. Chen, X. Wu, and A. Selloni, *Physical Review B* **83**, 245204 (2011).
- [84] R. M. Horneich, Y. Komett, R. Nolan, and I. Wanklyn, B. M. an Yaeger, *Physical Review B* **12**, 5094 (1975).
- [85] H. Schuchert and R. Hüfner, E. Faulhaber, *Zeitschrift für Physik* **222**, 105 (1969).